

This is a repository copy of Detecting piston ring—cylinder liner metal—metal contact in a fired large marine diesel engine using piezoelectric transducers.

White Rose Research Online URL for this paper: https://eprints.whiterose.ac.uk/id/eprint/225465/

Version: Accepted Version

Article:

Rooke, J. orcid.org/0000-0003-0720-7891, Li, X. and Dwyer-Joyce, R.S. (2025) Detecting piston ring—cylinder liner metal—metal contact in a fired large marine diesel engine using piezoelectric transducers. SAE International Journal of Engines, 18 (3). 03-18-03-0017. ISSN: 1946-3936

https://doi.org/10.4271/03-18-03-0017

© 2025 SAE International. This is an author-produced version of a paper subsequently published in SAE International Journal of Engines. Uploaded in accordance with the publisher's self-archiving policy.

Reuse

Items deposited in White Rose Research Online are protected by copyright, with all rights reserved unless indicated otherwise. They may be downloaded and/or printed for private study, or other acts as permitted by national copyright laws. The publisher or other rights holders may allow further reproduction and re-use of the full text version. This is indicated by the licence information on the White Rose Research Online record for the item.

Takedown

If you consider content in White Rose Research Online to be in breach of UK law, please notify us by emailing eprints@whiterose.ac.uk including the URL of the record and the reason for the withdrawal request.



Detecting piston ring-cylinder liner metal-metal contact in a fired large marine diesel engine using piezoelectric transducers

Abstract

Shear polarized ultrasonic sensors have been instrumented onto the outer liner surface of an RTX-6 large marine diesel engine. The sensors were aligned with the first piston ring at top dead center and shear ultrasonic reflectometry (comparing the variation in the reflected ultrasonic waves) was used to infer metal-metal contact between the piston ring and cylinder liner. This is possible as shear waves are not supported by fluids and will only transmit across solid-to-solid interfaces. Therefore, a sharp change in the reflected wave is an indicator of oil film breakdown. Two lubricant injection systems have been evaluated, pulse jet and needle lift type injectors. The needle lift type is a prototype injector design with a reduced rate of lubricant atomization relative to pulse jet injectors. This is manifested as a smaller reduction in the reflected ultrasonic wave, showing less metal-metal contact had occurred. During steady-state testing, the oil feed rate was varied; the high flow rate case was shown to reduce the amount of piston ring-liner contact, whilst no changes in the lubricant film thickness had previously been detected using traditional longitudinal ultrasonic sensors. This displays the increased sensitivity of shear sensors relative to longitudinal sensors in respect to the quantity of lubricant present. Piston ring oil film breakdown was also studied at a range of steady-state loading levels and engine slow-down, showing the amount of contact decreased as engine load decreased, providing a real-time indication of the lubrication regime of the piston rings. When the load was further decreased, into total shutdown of the engine, the amount of contact increased until the engine had stopped rotating. The study has demonstrated the capability of shear ultrasonic sensors to detect changes in solid contact caused by; injector design, oil feed rate, engine load, and engine shut down.

1 Introduction

Operational advancements in marine diesel engines focus on methodologies to raise engine efficiency whilst reducing parasitic losses. This is to meet emission legislation such as those set by the International Maritime Organization, to reduce greenhouse gas emissions by 40% by 2030 relative to 2008 emissions [1]. This is partially driven by the international shipping sector which contributes 2.2 % of anthropogenic CO₂ emissions [1] and marine diesel engines contributing a notable portion of those emissions. In internal combustion engines, 9-20% of the energy content in the fuel is wasted due to parasitic losses [2], [3], [4], and the greatest single contributor to this, is the piston ring pack (25% of frictional losses, [5]). The piston ring pack experiences the full range of the Stribeck Curve through each piston stroke: at the top dead centre (TDC) and the bottom dead centre (BDC), the instantaneous zero-velocity of the piston at these points leads to potential boundary lubrication whilst mid-stroke the high velocity of the piston enables a complete hydrodynamic film. Boundary lubrication of the piston ring, i.e. metal-metal contact between the piston ring and cylinder liner, is a significant contributor to ring pack friction and, hence wastage of the energy content in the fuel. Therefore, a large portion of ring pack friction occurs at either TDC or BDC.

Due to the nature of piston rings, being at the centre of internal combustion engines and being exposed to harsh operational conditions, the study of their lubrication regime and potential lack thereof lubricant film is inherently difficult. Scuffing of the piston rings/skirt has been the focus of several previous articles although they are limited to bespoke test rigs to simulate internal

combustion engine scuffing and study the ring/piston skirt surface post-test rig operation [6], [7], [8], [9], [10], [11], [12], [13], [14], [15]. These works are manually intensive and involve surface examination post testing and can provide useful insight into the progressive deterioration of the surfaces. However, the non-live nature surface examination limits their real-world applicability, and it provides no insight into how real operating conditions affect the lubrication regime. Alternatively, several works have simulated piston ring scuffing [16], [17], [18], [19] although the simulations are limit by the non-ideal validation methodologies of the surface examination previously mentioned. Therefore, the real-world applicability of scuffing measurements is limited and to date there are no works on piston ring-liner metal-metal contact during fired engine operation.

This article follows from the works by Rooke et al. [20], [21], [22] on the ultrasonic sensors that were instrumented on external cylinder liner surface of WinGD's RTX-6 test engine. In Rooke et al. [21] the longitudinal ultrasonic sensors were studied by applying the traditional ultrasonic reflectometry data processing methodology to produce oil film thickness measurements for each of the piston rings at several locations. The absolute minimum oil film thickness measured was 6.3 µm for the first piston ring at the TDC, however a range of anomalous trends were present in the data. Further research was conducted onto the data from the longitudinal ultrasonic transducers in Rooke et al. [22] into the anomalous trends found in Rooke et al. [21] which were found to be due to ultrasonic reflections from outside the measurement area being detected, leading to abnormal trends in the data. An alternative data processing technique by indexing the Hilbert envelope was applied to the data which removed the impact of the undesired ultrasonic reflections, leading to a greater measurement of the true oil film thickness, which was typically 20 % greater than those from the traditional data process technique. This research expands the previous works by applying the novel data processing methodology to the shear ultrasonic sensors instrumented onto the RTX-6 engine to study piston ring-liner metal-metal contact at a range of engine conditions.

2 Background

Ultrasonic reflectometry analysis is based upon the principle that as a wave propagating through a media impacts a discontinuity, there is a partial reflection/partial transmittance of that wave. This basis has been extensively used in various works to study piston ring oil film thickness [20], [21], [22], [23], [24], [25], [26], [27], [28], [29] and other tribological applications such as; journal bearings [30], [31], [32], [33], roller bearings [34], [35], [36], slipper bearings, [37] and O-ring seals [38]. The portion of the wave that is reflected is termed the reflection coefficient, R, and is dependent on the acoustic impedance mismatch between the media, see Equation 1. The acoustic impedance, z, is the product of the density and speed of sound.

$$R = \frac{z_2 - z_1}{z_2 + z_1}$$
 1

This equation holds for both longitudinal and shear ultrasonic waves (note that the speed of sound differs depending on the wave mode being propagated). The notable distinction between longitudinal and shear waves is that fluids are unable to support shear waves, therefore, longitudinal sensors may be used for oil film thickness measurements whereas shear sensors may not. Due to this, if a shear wave propagating through a solid media impacts a fully formed lubricating film, a complete reflection of the ultrasonic wave occurs and no discernible change

in the reflection coefficient is seen. Therefore, in the context of a shear ultrasonic sensor instrumented onto an engine liner, there would be no change in the reflection detected with crank angle (CA) if there was no metal-metal contact in the sensing region. In practice, shear ultrasonic waves can permit a small amount of transmission dependent on the viscosity of the fluid [39] although in those experiments, that transmission was negligible compared to that caused by solid contact.

Shear ultrasonic sensors can be used to measure several parameters; the acoustoelastic effect in the media, lubricant solidification, shear wave penetration, or metal-metal contact. In the context of the piston ring pack in internal combustion engines, the combustion pressure is not considered high enough for lubricant solidification. In the RTX-6, the peak combustion pressure is in the order of 200 bar whilst pressures in the order of giga pascals are required for solidification of the lubricant. Therefore, a sharp reduction in the reflection coefficient measured is either due to a shear wave penetrating through an extremely thin piston ring oil film or metal-metal contact between the piston/ring and liner. The two can be differentiated by calculation of the oil film penetration depth as shear waves are only capable of penetrating through a short distance (up to several microns). The penetration depth, δ , can be calculated using Equation 2 [40]. In which η , is the dynamic viscosity, ρ_l , is the density of the fluid and, f, is the central frequency of the transducer.

$$\delta = \sqrt{\frac{\eta}{\pi f \rho_l}}$$
 2

The application of shear ultrasonic reflectometry to the piston ring-cylinder liner interaction enables the identification of metal-metal contact between the two surfaces during fired operation of the engine. This can be achieved without any modification to the engine itself. Whilst previously, this could only be achieved through dismantling of the engine and observation of the two surfaces.

3 Test engine

This article covers fired testing on WinGD's two-stroke marine diesel RTX-6 test engine, shown in *Figure 1*. Several relevant parameters of the engine are given in *Table 1*.



Figure 1 RTX-6 test engine reproduced from [21].

Table 1 RTX-6 engine parameters, edited from [22].

Engine Parameter	Value	Unit	
Maximum power	6470	kW	
No. of cylinders	4	-	
Cylinder bore	500	mm	
Piston stroke	2250	mm	
Number of pulse jet	8	-	
injectors	O		
Number of needle lift	6	-	
type injectors	U		
Maximum rotational	105.5	rpm	
speed	103.3		

In this work two lubricant injector designs were evaluated; Pulse Jet (PJ) and Needle Lift Type (NLT). PJ injectors are commonly used injectors in marine engines, in which the main components of the system are shown in *Figure 2*. The dosage pump feeds lubricant to the injectors and is powered by servo oil from the marine diesel engines oil circuit. The lubricant feed rate and injection timing are controlled via a solenoid valve in the dosage pump which provides full flexibility in injection timing over the operation range of the engine.

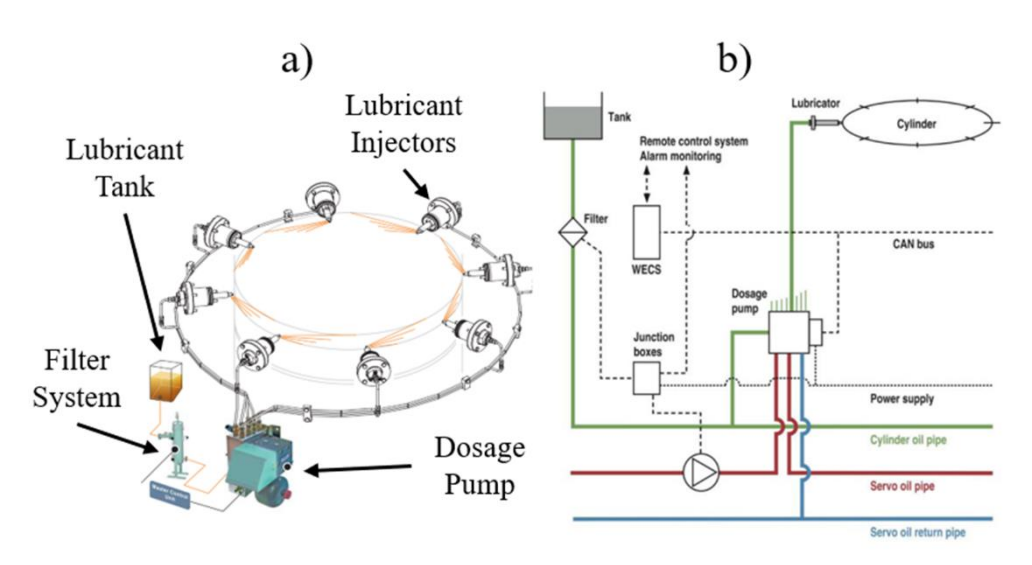


Figure 2 Pulse jet injector oil system. (a) Pulse jet injector components, reproduced from [21]; (b) Schematic of the complete system, reproduced from [22].

A disadvantage of the PJ system is that the atomisation rate of the lubricant varies between sequential lubricant sprays. This will lead to inconsistencies in the lubricant film over time. To overcome this, a prototype injection system was implemented, the NLT injectors, which were combined with a common rail system. The NLT injectors reduce, and have better control of, the rate of lubricant atomisation. Therefore, the NLT injectors have the potential to reduce lubricant consumption relative to PJ injectors. The NLT injection system is detailed in *Figure 3*. These injection systems have been evaluated in previous works (Rooke et al. [21], [22]) on the RTX-6 engine, in which a series of longitudinal ultrasonic transducers reviewed the PJ and NLT injection systems at the nominal oil flow rate (0.8 g/kWh), and the NLT injectors were

shown to typically increase the oil film thickness by 20 %. This increase in lubricant film thickness was achieved whilst oil loss to the exhaust manifold was reduced by 66.7 % [41].

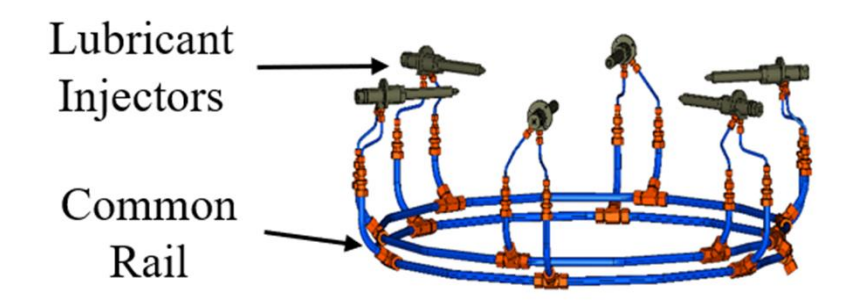


Figure 3 Needle lift type injectors, reproduced from [21].

The PJ and NLT injection systems have been used to define two engine configurations when the differing lubricant injection systems were used. Both injection systems had the same lubricant injection regime, leading to a lubricant distribution of 80% above the ring pack, 10% into, and 10% below.

The RTX-6 test engine was previously instrumented with a series of thermocouples down the cylinder liner, further details of the thermocouple locations are shown in Milanese et al [41]. A thermocouple was positioned in close proximity of the first piston ring at its TDC position, therefore, these temperature measurements were used to infer the temperature measurements over the sensing regions.

3.1 Ultrasonic instrumentation

Seven ultrasonic sensors were installed on the RTX-6 engine; five longitudinal (green circles) and two shear (red and yellow circles), as shown in Figure 4(a). The active element diameter of the ultrasonic transducers (the sensing area) was 14 mm, which is less than the width of any of the piston rings. Ultrasonic transducers provide an average measurement over the active element area, therefore, the width being less than the piston ring width enables a greater measure of the true reflected wave when a piston ring is aligned with the sensor.

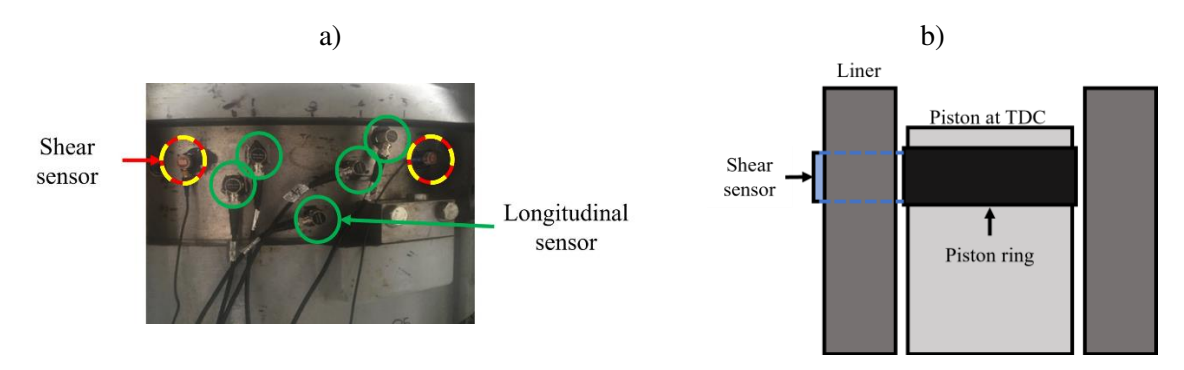


Figure 4 (a) Instrumented ultrasonic sensors, shear sensors are highlighted in red/yellow and longitudinal sensors in green (b) schematic diagram of the shear sensors relative to the first piston ring at its TDC position.

The ultrasonic sensors were bonded to the external liner surface by an industrial adhesive and magnetically clamped to the liner to enable curing of the adhesive overnight at room temperature. Critically, to instrument the sensors and perform the ultrasonic testing, no

modifications (other than some minor abrasive cleaning of the surface) to the marine diesel engine were made to conduct this testing.

This article focuses on the results for the two shear ultrasonic transducers, the data from the five longitudinal transducers has previously been discussed in Rooke et al. [21], [22]. The two shear ultrasonic sensors (red and yellow circles in *Figure 4(a)*) were aligned with the first piston ring at its TDC position as shown schematically in *Figure 4(b)*. The piston/piston ring position was aligned to the ultrasonic data via a shaft encoder to measure the CA.

A typical ultrasonic reflection in the time-domain is shown in *Figure 5*. Note that four ultrasonic reflections are shown and the amplitude decreases for sequential reflections as the signal attenuates. Furthermore, the ultrasonic reflection shown in *Figure 5* was from recorded with the piston significantly far away from the sensing area and when the liner was dry.

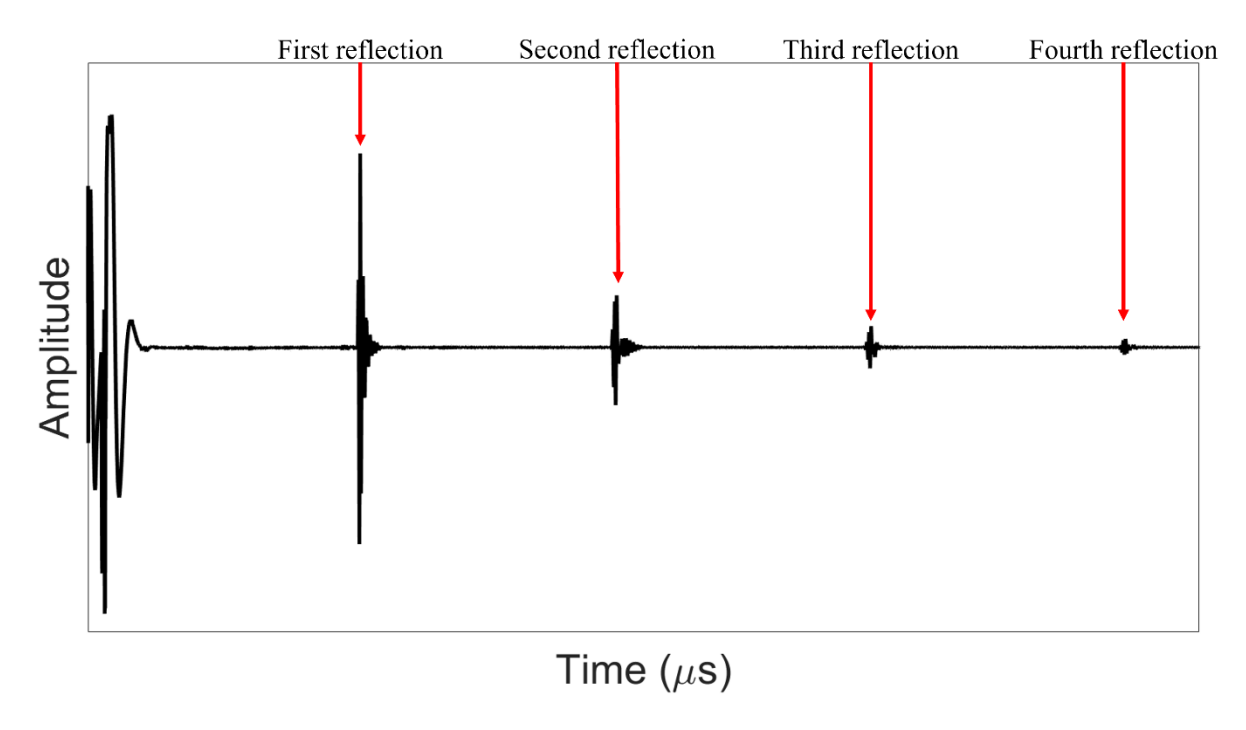


Figure 5 A typical time-domain (A-scan) reflection showing four reflections from the internal surface of an engine liner.

The ultrasonic signals were produced, received, and managed using an ultrasonic pulser receiver (UPR). The UPR contained a card to generate short voltage pulses which were sent to the ultrasonic sensors which, via the principle of piezoelectricity, converted the pulses to mechanical displacements and instigated a pressure wave in the cylinder liner. The wave propagated through the liner and was reflected from the internal surface/piston ring. The measurements were pulse-echo, i.e. the ultrasonic waves were pulsed and received by the same transducer. The sensor converted the wave back into a voltage that was digitised in the UPR. A bespoke LabVIEW interface was used to record and optimise the ultrasonic signals. The ultrasonic testing equipment is summarised in Figure 6 and the duration of each data capture was 5 seconds, this ensured multiple engine revolutions were in each capture, therefore, enabling averaging of the ultrasonic data.

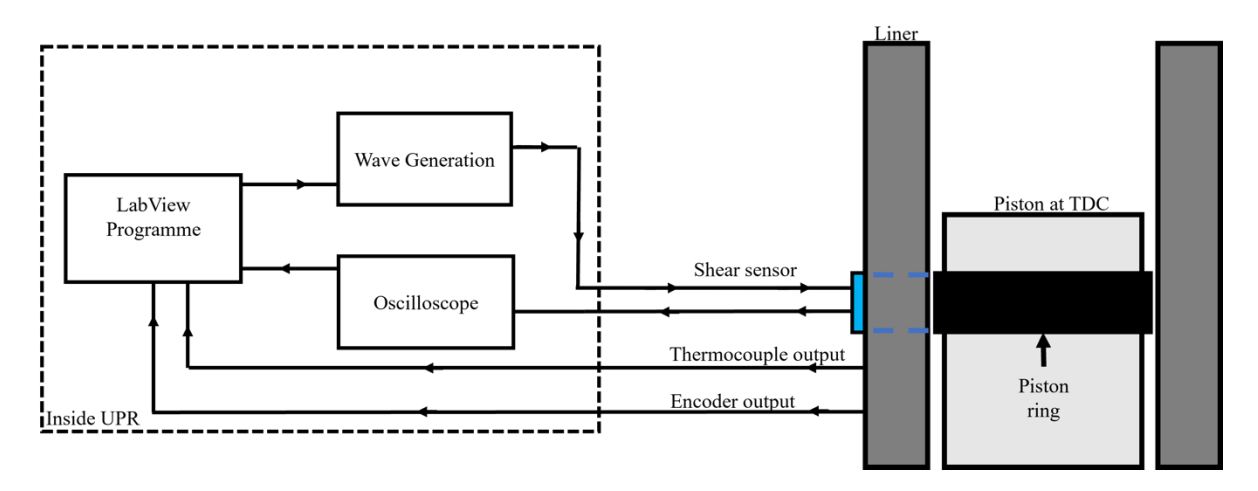


Figure 6 Schematic diagram of ultrasonic instrumentation.

3.2 Test conditions

Fired engine testing was performed at three steady-state loading levels: 100%, 50% and 25% each loading level was related to a different engine speed (105.5, 83.6 and 66.2 rpm respectively) and the engine loading cycle is shown in *Figure 7(a)*. The engine was not stopped between the different loading levels, therefore providing a period of un-steady operation when the engine loading was transitioning loading level. A full shut-down only occurred after 25% steady-state loading. Within each steady-state loading period, the set value of the oil feed rate was varied from its nominal position to vary the oil feed rate (nominal flow of 0.8 g/kWh) to a low flow (0.6 g/kWh) and high flow (1.2 g/kWh) over a 20-minute interval as shown in *Figure 7(b)*. The oil feed rate is proportional to the engine load, therefore, was the load decreased the quantity of oil injected proportionally decreases, as is standard for the engine.

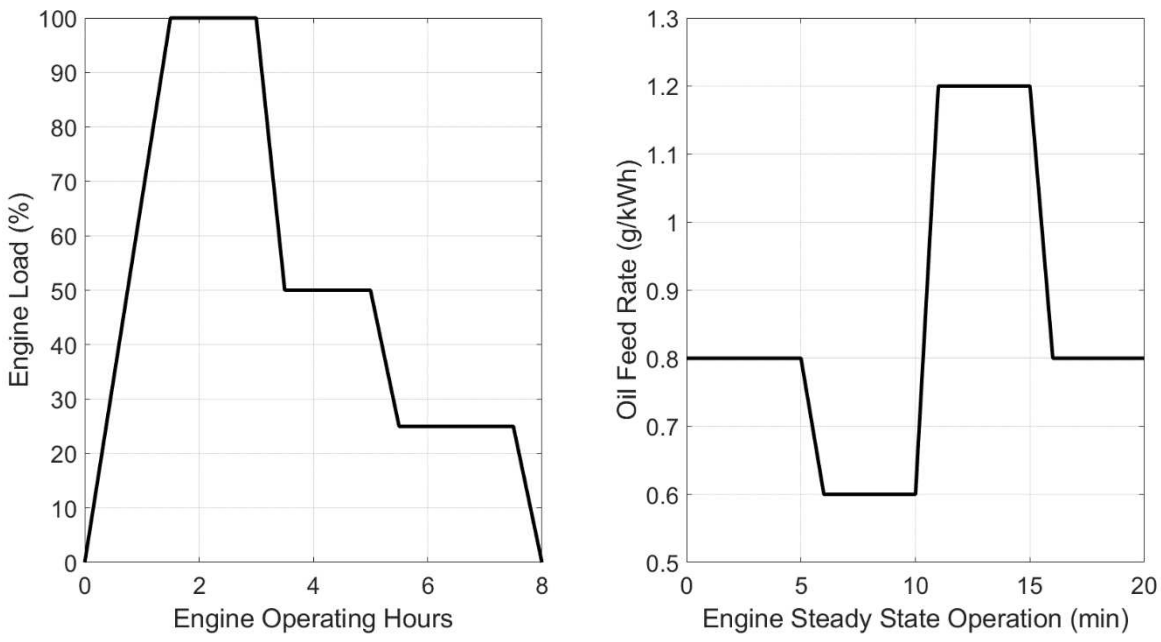


Figure 7 (a) Engine loading variation (b) Oil feed rate variation for each lubricant injection system, reproduced from [21].

3.3 Signal processing

The ultrasonic data was captured as a series of stacked time-domain reflections (i.e. an array of the first reflections shown in Figure 5), see Figure 8(a)-(b). To convert these measurements into reflection coefficient, the ultrasonic reflection of interest was isolated, and the Hilbert envelope was overlayed. Furthermore, the peak of the Hilbert envelope was normalised relative to a reference envelope to provide the reflection coefficient. A reference envelope was defined for each data capture from the mean reflection when the piston ring was significantly far from the measurement zone, see the red box in Figure 8(a). Whereas the variation in the time-domain response from a typical aligned piston ring is shown in the blue box of Figure 8(a). In most ultrasonic reflectometry oil film thickness measurements, the reflection coefficient is defined from a frequency index of the ultrasonic reflection in the frequency domain. However, in a previous work by Rooke et al. [29], the Hilbert envelope-based methodology was shown to be significantly less impacted by ultrasonic reflections from outside the measurement region, leading to a greater representation of the true reflection coefficient. The Hilbert envelope methodology is expected to be superior to a frequency-domain frequency index in this application due to the relatively long propagation distance through the RTX-6 cylinder liner enabling a greater spread of the ultrasonic waves.

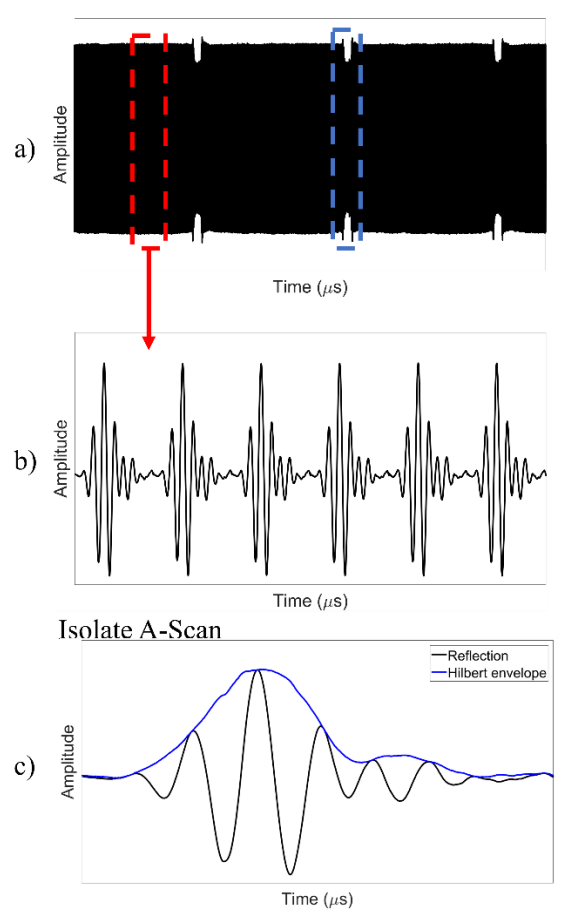


Figure 8 (a) Raw ultrasonic data. (b) Zoomed version of Figure 8(a). (c) Isolated timedomain reflection with the signal's Hilbert envelope overlayed.

4 Reflection coefficient variation

The reflection coefficient variation for a shear sensor aligned with the top piston ring at the TDC for 100% loading steady-state engine operation (nominal oil feed rate) for the two lubricant injection systems is shown in *Figure 9*. The region where the piston ring was aligned over the shear sensor is highlighted in the blue region.

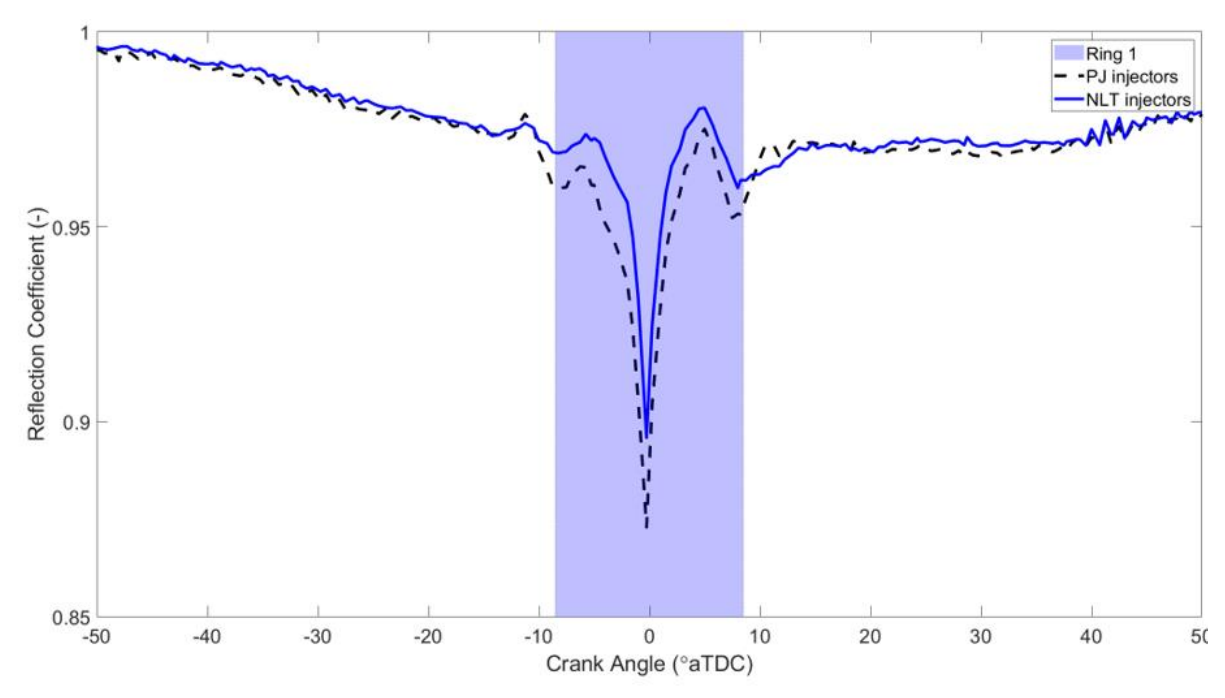


Figure 9 Reflection coefficient variation from a shear sensor at steady-state 100% loading for two injector systems (the blue region indicated where the piston ring was aligned over the sensor).

Over the CA range displayed, the shear sensor in *Figure 9* sees a progressive reduction in the reflection coefficient reaching 0.97 on either side of the piston ring alignment region. This is theorised to be due to this sensor being polarised circumferentially and experiencing an acoustoelastic effect as the temperature and pressure inside the combustion chamber varies. A combination of this sensor, and a sensor polarised radially and axially may enable multi-dimensional stress measurements, similar to those seen in the cold rolling of steel [42].

Whilst over the piston ring alignment region (-8.5° to 8.5° CA) a sharp reduction in reflection coefficient is seen for both lubricant injection systems, reducing to 0.87 for the PJ injectors at -0.25° CA. Due to shear waves inability to propagate through a fully formed, greater than several micron, lubricant film, this sharp reduction is either the shear wave penetrating through an extremely thin film or piston ring-liner metal-metal contact.

The magnitude of the reduction in reflection coefficient is different for the two lubricant injection systems, the NLT injectors, with the reduced rate of lubricant atomisation, led to a smaller reduction (0.9, versus 0.87 for the PJ injectors). Indicative that the NLT injectors either led to a reduction in piston ring metal-metal contact or a thicker lubricant film enabling less of the shear wave to penetrate through. This finding agrees with the results from the longitudinal sensors instrumented on the RTX-6 engine discussed in Rooke et al. [21], [22], that the reduction in lubricant atomisation provided thicker lubricant films. It was shown that the minimum oil film thickness when using the NLT injectors over the first piston ring was 7.4 µm whilst it was 6.3 µm for the PJ injectors, a near 20 % increase for the prototype injector design. A closer inspection of each engine cycle that produced the summary figure in *Figure 9* is shown in *Figure 10* for the PJ injectors and NLT injectors in subplots (a) and (b) respectively.

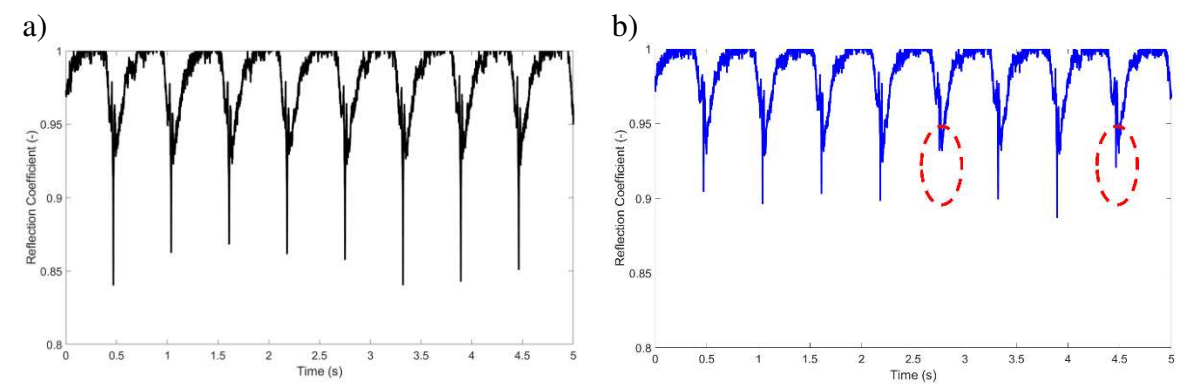


Figure 10 Reflection coefficient variation over a complete data capture (a) PJ injectors, (b) NLT injectors.

The varying rates of lubricant atomisation are directly visible in the raw reflection coefficient data. For the PJ injectors, ($Figure\ 10(a)$) which has the higher rate of lubricant atomisation, there is a sharp drop in reflection coefficient for each engine cycle with the minimum value varying between 0.84-0.87. Whilst for the NLT injectors, ($Figure\ 10(b)$), the lower rate of lubricant atomisation, the minimum value varies between 0.89-0.91 with two revolutions showing no sizeable drop equivalent the other engine cycles, see the red circles in $Figure\ 10(b)$. These figures indicate that the shear wave penetration/piston ring metal-metal contact is occurring in each revolution of the engine for the PJ injectors. Whilst for the NLT injectors, when thicker oil films were measured [21], [22], the extent of shear wave penetration/metal-metal contact was definitively reduced with some revolutions having major reductions. Further indicating the beneficial lubrication regime of the top piston ring at the TDC when using the NLT injectors.

To discern whether the drop in reflection was either metal-metal contact or shear wave penetration, the oil film penetration depth can be quantified using Equation 2. To calculate this, the viscosity of the oil was required, therefore, engine oil was scavenged from the RTX-6 engine during 100% steady-state operation during testing on the PJ injectors. The scavenged oil enables a more representative measure of the engine oils viscosity due to its exposure to contaminants such as combustion and wear products. A Brookfield viscometer was used to determine the viscosity of the engine lubricant at specified temperatures, T, to define the degraded oils Vogel Equation, Equation 3, an equation that represents the viscosity variation with temperature. The coefficients of the Vogel Equation for the RTX-6 scavenged engine lubricant are shown in Table 2.

$$\eta = A \times \exp\left(\frac{B}{T - C}\right)$$

Table 2 Vogel Equation coefficients.

Coefficient	Value
A	5.04 x 10 ⁻¹¹
В	1395.3
С	-423.0

Applying the Vogel Coefficients of *Table 2* to Equation 3 in combination with temperature measurements from the internal surface of the cylinder liner in close proximity of the first piston ring at the TDC, the lubricant viscosity at 100% loading steady-state operation was found to be 0.15 cP. Using this dynamic viscosity in Equation 2, the shear wave penetration depth was calculated to be 0.25 μm. Whereas, the oil film thickness measurements in the RTX-6 from Rooke et al. [21], [22], had an absolute minimum oil film thickness of 6.3 μm from either injection system (PJ or NLT injectors) or data processing methodology (Frequency index or Hilbert Envelope) for the top piston ring during 100% loading steady-state operation. Therefore, the shear wave penetration depth is a factor of 30 less than the minimum recorded film thickness, showing that a shear wave would have been unable to penetrate through to a piston ring aligned parallel to the cylinder liner if a fully formed lubricant film had been achieved (Figure 11(a)).

Due to the averaging effect of ultrasonic transducers over the measurement region, in theory, if the piston ring was found to have significantly rotated it would enable the possibility of an average minimum oil film thickness of 6.3 μ m whilst the true minimum oil film thickness is less than 0.25 μ m (Figure 11 (b)). This would enable the minimum oil film thickness measurements seen in Rooke et al. [21], [22] whilst a shear wave could penetrate through a very thin oil film (>0.25 μ m). For identification of whether both factors may be true a worst-case scenario is considered, a rectangular piston ring that is free to rotate (note that the piston rings in the RTX-6 are barrel shaped and piston ring wear is typically in the centre of the ring, not the edges, therefore, a rotation such as considered here would be atypical).

Consider the case of the PJ injectors, a minimum reflection coefficient of 0.84 was measured, yet this lubricant injection system had an absolute minimum oil film thickness of 6.3 μ m. Under the assumption that 16 % of the piston ring was closer than 0.25 μ m from the liner (to enable a reflection coefficient of 0.84), and assuming a rectangular geometry of ring, it would require a true minimum oil film thickness of -2.3 μ m (Figure 11(c)). Indicating that 16 % of the ultrasonic wave could not have penetrated through to the piston ring, without metal-metal contact also occurring. Therefore, the sharp reductions in reflection coefficient in Figure 9 and Figure 10 are at least due to a partial metal-metal contact between the piston ring and cylinder liner, i.e., the lubricant film breaking down at the TDC and boundary lubrication occurring.

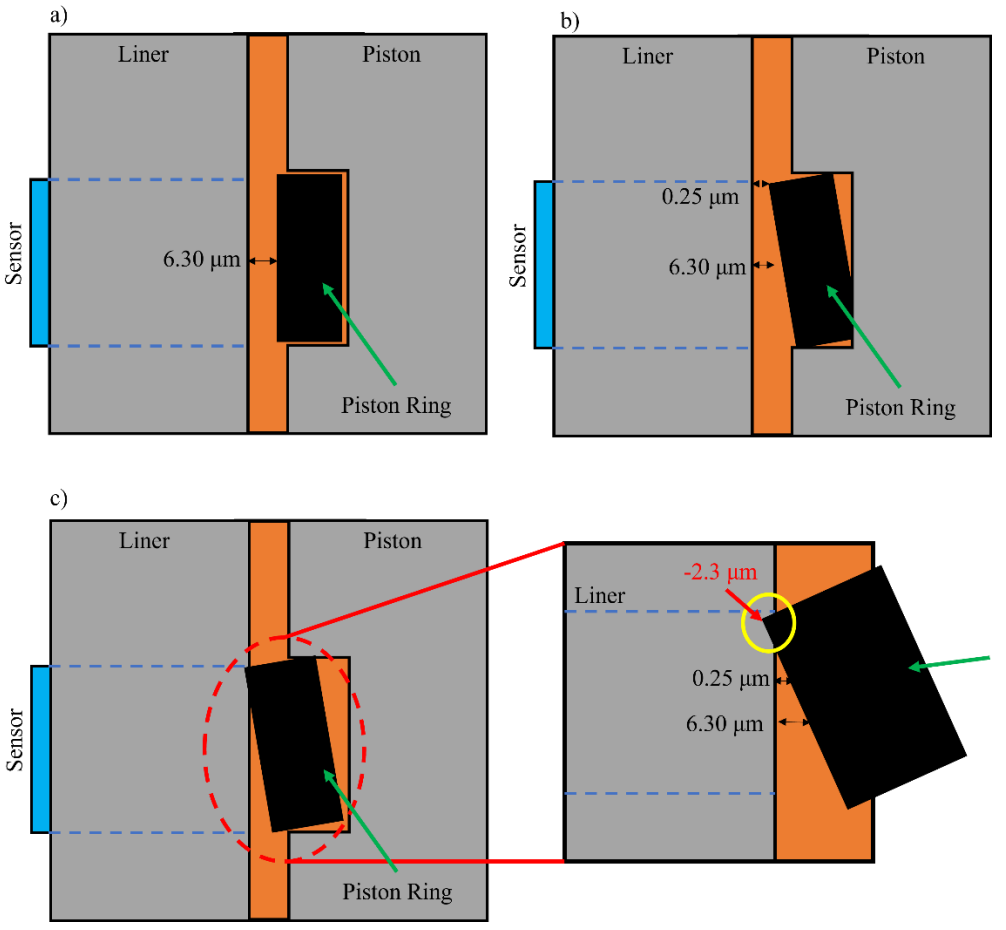


Figure 11 Piston ring minimum oil film thickness scenarios (a) parallel piston ring, (b) angled piston ring with a true minimum of $0.25~\mu m$ (c) angled piston ring with 16~% of the piston ring face under the shear wave penetration depth $(0.25~\mu m)$.

4.1 Oil feed rate variation

Within each steady-state loading period the oil feed rate was varied from the nominal rate to a high and low flow rate in five-minute intervals as previously shown in Figure 7(b). The reflection coefficient using the NLT injectors for an engine revolution at the centre of each feed rate interval is presented in Figure 12.

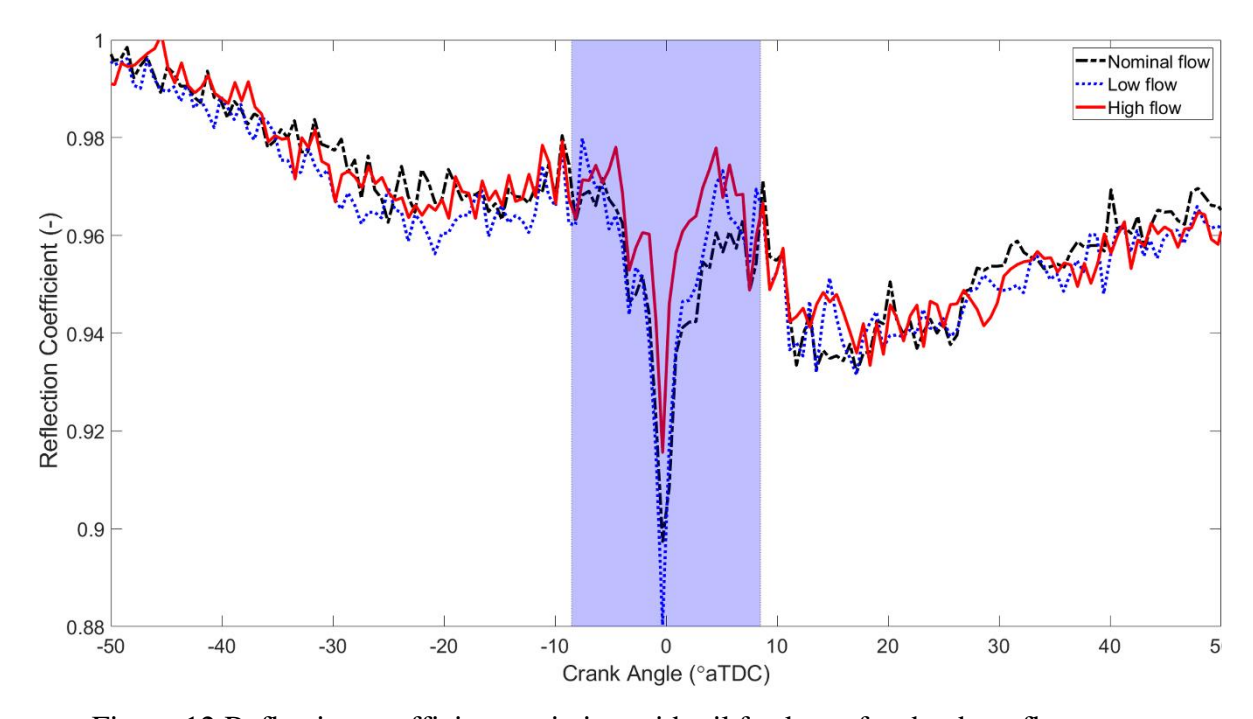


Figure 12 Reflection coefficient variation with oil feed rate for the three flow rates considered.

The initial study of *Figure 12* shows likewise trends in the reflection coefficient for the three oil feed rates, and similar to those seen for the two injection systems in *Figure 9*. Closer inspection on the TDC region, the blue region of *Figure 12*, displays that the higher flow rate of lubricant led to the general trend of a greater reflection coefficient (0.92) than those of nominal (0.90) or low flow rate (0.88). Consequently, indicating that as expected, when more oil was injected onto the cylinder liner, less metal-metal contact between the piston ring and liner was detected. Therefore, the shear ultrasonic sensors could identify variations in oil feed rates which were conducted in 5-minute intervals.

The minimum oil film thickness from the longitudinal sensor aligned with the first piston ring at the TDC was reviewed in Rooke et al. [21] in which no identifiable change in oil film thickness with oil feed rate was seen. However, as the shear sensors showed a minor reduction in metal-metal contact over the same period, it indicates that shear sensors appear to provide a more sensitive measure of the quantity of lubricant present than longitudinal sensors. This is likely due to shear waves being unable to propagate through fluids. It is worth noting that the oil feed rate variation was only in 5-minutes intervals, a longer variation period would likely have produced a more discernible change in metal-metal contact as the liner was progressively starved of lubricant.

4.2 Loading comparison

Through the fired engine testing, three steady-state loading steps were studied, the reflection coefficient over the steady-state period for the nominal oil feed rate is shown in Figure 13 for the NLT injectors.

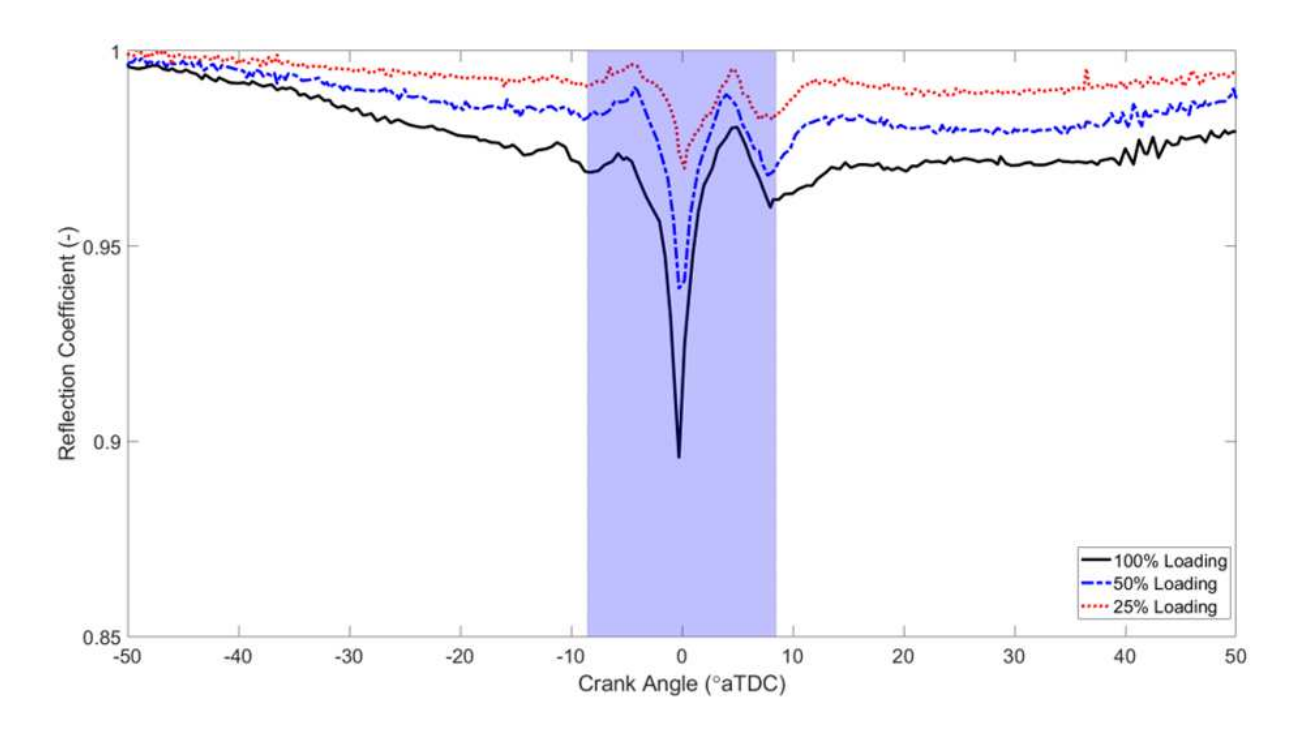


Figure 13 Reflection coefficient variation with engine loading for the NLT injectors.

The impact of the variation in engine loading on piston ring/liner metal-metal contact is shown in *Figure 13*, with a reduction in engine loading reducing the contact between the piston ring and cylinder liner. From 100% to 25% loading there was a 71% reduction in the magnitude of the reflection coefficient drop, indicating a significant reduction in metal-metal contact. A reduction in metal-metal contact at lower loading levels is expected, as at lower loading there is a reduction in combustion pressure and, therefore, less piston ring radial load and conformity between the ring and liner. This further agrees with previous work on the RTX-6 test engine, that as the load was lowered on the engine the minimum oil film thickness increased. For example, the minimum oil film thickness for the NLT injectors increased from 7.4 μ m at 100% loading, to 8.1 μ m at 50% loading and 10.4 μ m at 25% loading [21]. Critically though, based on previous analysis, one may assume that there would not be metal-metal contact if oil films with a minimum of 10 μ m were detected although this is evidently not the case.

4.3 Engine slow-down

The continuous operation of the engine between the loading levels provided intervals of varying engine loading/speed. In the case of the engine moving from 50% to 25% loading, a 44-minute period, ultrasonic reflections were captured for 5 seconds every minute. The minimum reflection coefficient from each engine cycle for the NLT injectors and the corresponding engine rotational speed is shown in *Figure 14*. Note that this test used the nominal oil feed rate of 0.8 g/kWh.

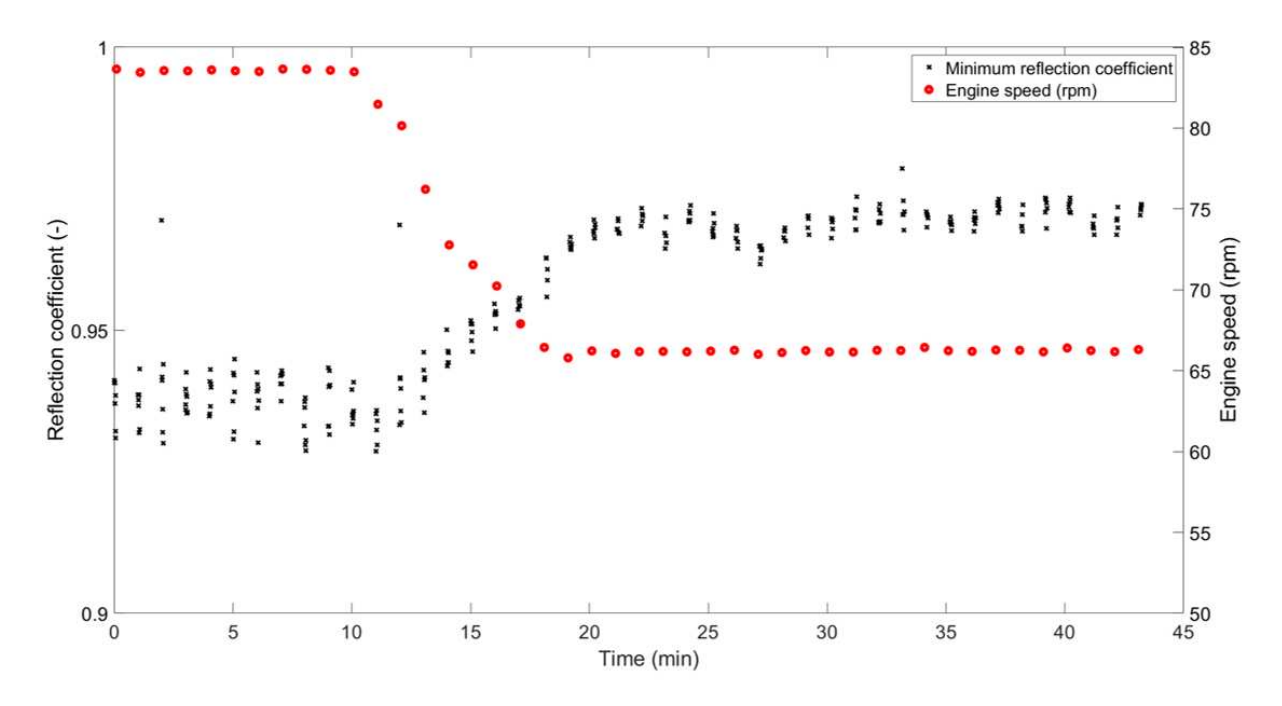


Figure 14 Minimum reflection coefficient as engine loading decreased from 50% to 25% for the NLT injectors.

The engine slow-down minimum reflection coefficient (*Figure 14*) shows agreeing results to *Figure 13*, that a reduction in engine load lessens the metal-metal contact occurring. The minimum reflection coefficient varies from 0.93 when at 50 % loading (83 rpm) to 0.97 at 25 % loading (66 rpm), a halving of the relative contact between the two surfaces. This displays the ability of the shear sensors to provide a real-time representation of the lubrication regime of the piston ring pack.

It is worth noting that as internal combustion engines are highly complex systems, the reduction in engine load on the RTX-6 results in a range of parameters being affected, such as combustion pressure, quantity of lubricant injected, engine rotational speed amongst many others. The methodology used here cannot separate the impact from individual factors on the metal-metal contact, but it provides a summary of the overall system impact.

4.4 Engine shut-down

At the end of testing each lubricant injector system, the RTX-6 engine experienced a full shutdown from 25% loading. The reflection coefficient over these engine cycles is shown in *Figure 15* for the final 20 seconds of engine operation of the NLT injectors. Note that this test used the nominal oil feed rate of 0.8 g/kWh.

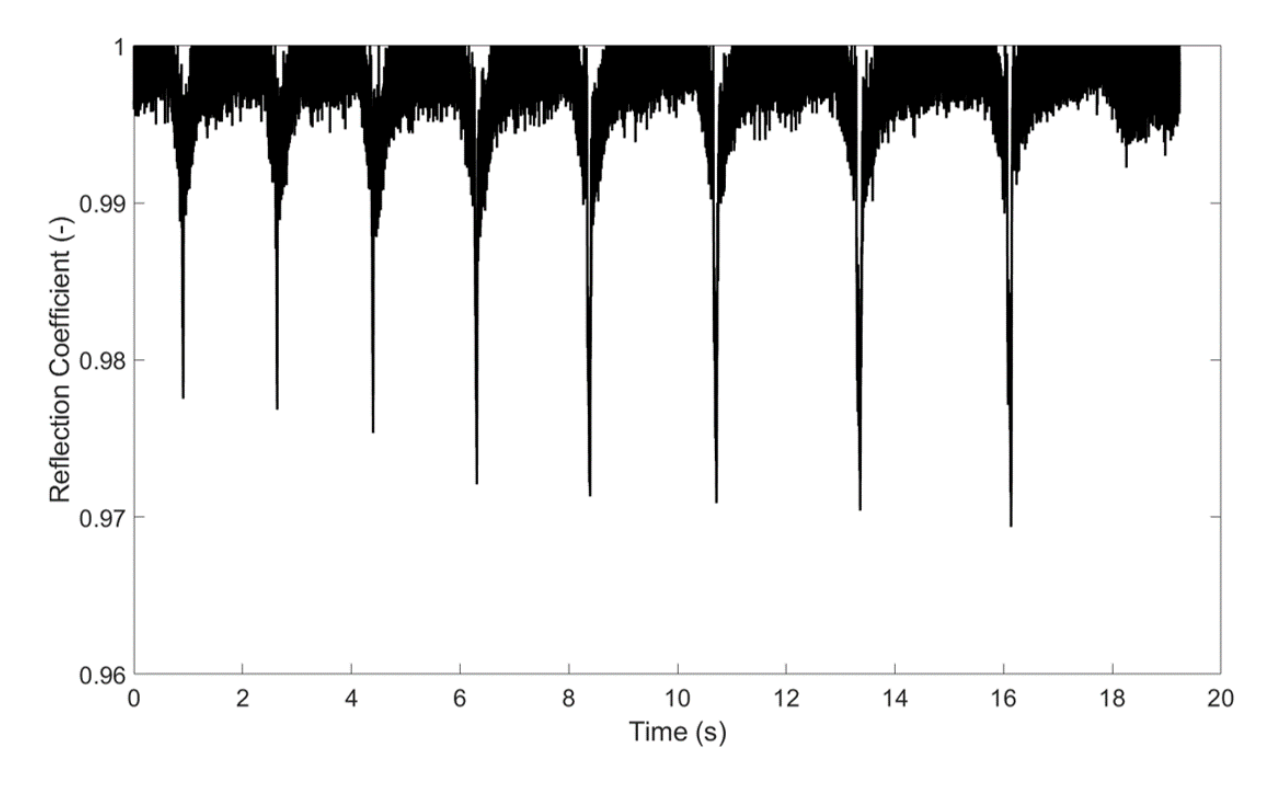


Figure 15 Reflection coefficient as the engine was shut-down from 25% loading.

Shut-down testing should be considered separately to those from changing engine loading as the engine is experiencing a different operational phase. Primarily, when the engine moves between loading levels (e.g. 100% to 50%), the load on the piston rings and factors such as the oil feed rate proportionally reduce but remain within the standard operating range. Whilst the shut-down tests cover the region where the lubricant injection system is at its minimum oil feed rate during operation, therefore, a reduction of lubricant present on the liner is not unexpected. Previously, in the engine slow-down results (*Figure 14*), as the load decreased the piston ring metal-metal contact decreased, whereas for a further load reduction (into full shut-down), the lubricant injection system further reduced the lubricant injected which led to the amount of piston ring metal-metal contact increasing as there was insufficient oil to lubricate the piston rings. This is shown via the progressive reduction in the minimum reflection coefficient for each engine revolution (0.978 to 0.968 over the 20 second shut down). The reduction in engine speed is also visualised by the increased timespan between the metal-metal contact (dips in the reflection coefficient).

5 Discussion

A combination of the slow-down and shut-down tests in terms of piston ring metal-metal can be summarised as: A reduction in engine loading reduces the amount of metal-metal between the first piston ring at the TDC and cylinder liner until the lubricant injection system is at its minimum operating levels. Once operating at its minimum level, this change in phase results in the piston ring metal-metal contact increasing as less lubricant is present to form a full oil film and increases until the engine has stopped rotating.

In previous research (Rooke et al. [21], [22]) longitudinal ultrasonic sensors have quantified the oil film thickness between the piston ring and cylinder liner in a fired RTX-6, a large diesel marine engine. This article has expanded how the piston ring oil films are studied by using shear ultrasonic sensors aligned with the first piston ring at its TDC position, which has shown

metal-metal contact to occur at a range of engine conditions. However, in previous research on this dataset (Rooke et al. [21], [22]) as well as previous ultrasonic based research into piston ring oil film thickness measurements ([23], [24], [25], [26], [27], [28], [29]) it has been assumed that the spring model [43] is applicable for calculation of oil film thickness. This model assumes that there are two parallel surfaces that are separated by a fully formed oil film which has been demonstrated to not be true in the case of the RTX-6. Instead, a mixed-mode lubrication regime should be considered to determine the true oil film thickness, such as that previously suggested by Dwyer-Joyce et al [44] and further explored in Cao-Romero-Gallegos et al. [45] although further research is required to realise this mixed-mode modification.

6 Conclusions

A WinGD test engine, an RTX-6, has been instrumented with a series of ultrasonic sensors. This article covered the shears sensors aligned with the first piston ring it's the top dead centre position. Shear sensors instigate transverse waves in a media and are therefore unable to propagate through bulk fluids, hence a change in the reflection observed by a shear sensor is indicative of three potential factors: lubricant solidification, a shear wave penetrating through a very thin oil film (up to several microns) or metal-metal contact. The pressures in internal combustion engines are not considered high enough to cause lubricant solidification and the shear wave penetration depth was found to be a factor of 30 less than the minimum lubricant film thickness measured in the engine. Thus, indicating the change in the reflection coefficient observed by the shear sensors to at least be partially due to metal-metal contact of the piston ring-cylinder liner.

Two lubricant injection systems were tested, pulse jet and needle lift type injectors. The prototype needle lift injectors, with a reduced rate of lubricant atomisation, were found to reduce the amount of piston ring metal-metal contact relative to the pulse jet injectors. The lubricant feed rate was varied during steady-state operation and the high flow rate case was found to provide a minor reduction in the amount of metal-metal contact compared to the nominal and low flow rate cases, this was found whilst no observable change in the minimum oil film thickness had been detected using longitudinal ultrasonic sensors. Metal-metal contact between the ring and liner has also been studied at three loading levels and slow-down testing, showing that as the engine load decreased, the metal-metal contact also proportionally decreased. Shut-down testing has provided differing findings from the slow-down tests as the engine was at its minimum operating conditions, this led to the amount of piston ring liner contact increasing until the engine stopped rotating.

This work has indicated how shear ultrasonic sensors can be used to identify when contact occurs between a piston ring and cylinder liner as well as the influence of both injector design and engine operating conditions. This has potential both as a device to support engine design, and as a sensor for implementation in a control algorithm to optimise engine lubrication to avoid metal-metal contact and to minimise emissions.

Acronyms

Bottom Dead Centre
Crank Angle

BDC	Bottom Dead Centre	
CA	Crank Angle	
NLT	Needle Lift Type	
PJ	Pulse Jet	

Acronyms

TDC	Top Dead Centre
UPR	Ultrasonic Pulser Receiver

Nomenclature

Symbol	Description	Unit
f	Frequency	MHz
R	Reflection coefficient	-
Z	Acoustic impedance	Pa.s.m ⁻²
δ	Penetration depth	μm
η	Dynamic viscosity	Pa.s
$\overline{ ho_l}$	Density of the fluid	kg.m ⁻³

References

- [1] International Maritime Organization, "Resolution MEPC.304(72) Initial IMO Strategy on Reduction of GHG Emissions from Ships and Existing IMO Activity Related to Reducing GHG Emissions in the Shipping Sector," 2018.
- [2] S. C. Tung and M. L. McMillan, "Automotive Tribology Overview of Current Advances and Challenges for the Future," *Tribol Int*, vol. 37, no. 7, pp. 517–536, 2004, doi: 10.1016/j.triboint.2004.01.013.
- [3] D. E. Richardson, "Review of Power Cylinder Friction for Diesel Engines," *J Eng Gas Turbine Power*, vol. 122, no. 4, pp. 506–519, 2000, doi: 10.1115/1.1290592.
- [4] P. Nagar and S. Miers, "Friction between Piston and Cylinder of an IC Engine: a Review," SAE Technical Paper 2011-01-14, 2011, doi: 10.4271/2011-01-1405.
- [5] J. Beulshausen, S. Pischinger, and M. Nijs, "Drivetrain Energy Distribution and Losses from Fuel to Wheel," *SAE International Journal of Passenger Cars Mechanical Systems*, vol. 6, no. 3, pp. 1528–1537, 2013, doi: 10.4271/2013-01-9118.
- [6] M. Shuster, D. Combs, K. Karrip, and D. Burke, "Piston ring cylinder liner scuffing phenomenon studies using acoustic emission technique," *Journal of Fuels and Lubricants*, vol. 109, pp. 901–913, 2000, doi: 10.4271/2000-01-1782.
- [7] P. Obert, T. Müller, H. Füßer, and D. Bartel, "The influence of oil supply and cylinder liner temperature on friction, wear and scuffing behavior of piston ring cylinder liner contacts A new model test," *Tribol Int*, vol. 94, pp. 306–314, 2016, doi: 10.1016/j.triboint.2015.08.026.
- [8] R. Zhang, Q. Zou, G. Barber, B. Zhou, and Y. Wang, "Scuffing Test Rig for Piston Wrist Pin and Pin Bore," SAE Int J Fuels Lubr, vol. 8, no. 1, pp. 16–20, 2015, doi: 10.4271/2015-01-0680.
- [9] W. Zhang, E. Becker, Y. Wang, Q. Zou, B. Zhou, and G. C. Barber, "Investigation of scuffing resistance of piston rings run against piston ring grooves," *Tribology Transactions*, vol. 51, no. 5, pp. 621–626, 2008, doi: 10.1080/10402000802044316.
- [10] C. Zhang, H. S. Cheng, and Q. J. Wang, "Scuffing behavior of piston-pin/bore bearing in mixed lubrication—part ii: Scuffing mechanism and failure criterion," *Tribology Transactions*, vol. 47, no. 1, pp. 149–156, 2004, doi: 10.1080/05698190490279100.

- [11] C. Zhang, H. S. Cheng, L. Qiu, K. W. Knipstein, and J. Bolyard, "Scuffing behavior of piston-pin/bore bearing in mixed lubrication—part i: experimental studies," *Tribology Transactions*, vol. 46, no. 2, pp. 193–199, 2003, doi: 10.1080/10402000308982616.
- [12] Z. Ma, R. Huang, X. Yuan, Y. Shen, and J. Xu, "Tribological performance and scuffing behaviors of several automobile piston rings mating with chrome-plated cylinder liner," *Friction*, vol. 10, no. 8, pp. 1245–1257, Aug. 2022, doi: 10.1007/s40544-021-0530-4.
- [13] T. Markut, F. Summer, M. Pusterhofer, and F. Grün, "Emergence of Coated Piston Ring Scuffing Behavior on an Application-Oriented Tribological Model Test System," *Lubricants*, vol. 12, no. 6, p. 218, Jun. 2024, doi: 10.3390/lubricants12060218.
- [14] J. Gussmagg, M. Pusterhofer, F. Summer, and F. Grün, "Experimental visualization of the wear and scuffing evolution of a flake graphite cast iron cylinder liner," *Wear*, vol. 526–527, p. 204948, Aug. 2023, doi: 10.1016/j.wear.2023.204948.
- [15] S. D. Fayaz and M. F. Wani, "Evaluating Scuffing Failure in Dry Sliding Conditions of Monolayer Chromium Piston Ring/Bulk Grey Cast Iron Liner Interface," *Tribology Online*, vol. 15, no. 1, pp. 9–17, Jan. 2020, doi: 10.2474/trol.15.9.
- [16] T. Kobayashi, "Prediction of Piston Skirt Scuffing via 3D Piston Motion Simulation," SAE Technical Papers, 2016, doi: 10.4271/2016-01-1044.
- [17] K. Sato, K. Fujii, M. Ito, and S. Koda, "Application to engine development of friction analysis by piston secondary motion simulation in consideration of cylinder block bore distortion," *SAE Technical Papers*, 2006, doi: 10.4271/2006-01-0428.
- [18] S. Dahdah, N. Biboulet, A. Lubrecht, and P. Charles, "Scuffing initiation caused by local starvation in a piston ring cylinder liner contact," *Tribol Int*, vol. 172, p. 107616, Aug. 2022, doi: 10.1016/j.triboint.2022.107616.
- [19] S. Dahdah, "Scuffing initiation prediction in a lubricated piston ring cylinder liner contact," Université de Lyon, Lyon, 2022.
- [20] J. Rooke, "Ultrasonic Measurements of the Piston Ring Lubricant Film Thickness in Three Different Sized Engines," University of Sheffield, Sheffield, 2021.
- [21] J. Rooke, X. Li, H. Brunskill, M. Stark, and R. Dwyer-Joyce, "Comparison of Ring-Liner Oil Film Thickness Resulting from Different Injector Designs in a Diesel Marine Engine Using an Ultrasound Measurement Method," *SAE Int J Engines*, vol. 14, no. 6, pp. 03-14-06–0053, May 2021, doi: 10.4271/03-14-06-0053.
- [22] J. Rooke, X. Li, and R. S. Dwyer-Joyce, "Applying the Hilbert Envelope Method to Refine the Ultrasonic Technique for Piston Ring Oil Film Thickness Measurements in a Marine Diesel Engine," SAE Int J Engines, vol. 16, no. 2, pp. 03-16-02–0011, Apr. 2022, doi: 10.4271/03-16-02-0011.
- [23] R. S. Mills, E. Y. Avan, and R. S. Dwyer-Joyce, "Piezoelectric Sensors to Monitor Lubricant Film Thickness at Piston—Cylinder Contacts in a Fired Engine," *Proceedings of the Institution of Mechanical Engineers, Part J: Journal of Engineering Tribology*, vol. 227, no. 2, pp. 100–111, 2012, doi: 10.1177/135065011246483.
- [24] R. Mills and R. Dwyer-Joyce, "Ultrasound for the Non-Invasive Measurement of IC Engine Piston Skirt Lubricant Films," *Proceedings of the Institution of Mechanical Engineers, Part J:*

- *Journal of Engineering Tribology*, vol. 228, no. 11, pp. 1330–1340, 2014, doi: 10.1177/1350650114538616.
- [25] R. Mills, "Ultrasonic measurement of lubricant films generated at the piston-cylinder interface of internal combustion engines," University of Sheffield, 2012.
- [26] R. Mills, J. Vail, and R. Dwyer-Joyce, "Ultrasound for the Non-Invasive Measurement of Internal Combustion Engine Piston Ring Oil Films," *Proceedings of the Institution of Mechanical Engineers, Part J: Journal of Engineering Tribology*, vol. 229, no. 2, pp. 207–215, 2015, doi: 10.1177/1350650114552538.
- [27] R. Mills, E. Y. Avan, and R. S. Dwyer-Joyce, "Measuring Lubricant Films at the Piston-Cylinder Contact: An Overview of Current Technologies with Focus on Ultrasound," *SAE Technical Paper 2013-01-0294*, 2013, doi: 10.4271/2013-01-0294.
- [28] E. Y. Avan, R. Mills, and R. S. Dwyer-Joyce, "Ultrasonic Imaging of the Piston Ring Oil Film During Operation in a Motored Engine Towards Oil Film Thickness Measurement," *SAE Int J Fuels Lubr*, vol. 3, pp. 786–793, 2010, doi: 10.4271/2010-01-2179.
- [29] J. Rooke *et al.*, "Piston ring oil film thickness measurements in a four-stroke diesel engine during steady-state, start-up and shut-down," *International Journal of Engine Research*, vol. 24, no. 4, pp. 1499–1514, Apr. 2023, doi: 10.1177/14680874221088547.
- [30] S. Beamish, X. Li, H. Brunskill, A. Hunter, and R. Dwyer-Joyce, "Circumferential film thickness measurement in journal bearings via the ultrasonic technique," *Tribol Int*, vol. 148, p. 106295, Aug. 2020, doi: 10.1016/j.triboint.2020.106295.
- [31] S. Beamish and R. S. Dwyer-Joyce, "Experimental Measurements of Oil Films in a Dynamically Loaded Journal Bearing," *Tribology Transactions*, vol. 65, no. 6, pp. 1022–1040, Nov. 2022, doi: 10.1080/10402004.2022.2106926.
- [32] S. Beamish, T. Reddyhoff, A. Hunter, and R. S. Dwyer-Joyce, "A method to determine acoustic properties of solids and its application to measuring oil film thickness in bearing shells of unknown composition," *Measurement*, vol. 195, p. 111176, May 2022, doi: 10.1016/j.measurement.2022.111176.
- [33] S. Beamish, T. Reddyhoff, A. Hunter, and R. S. Dwyer-Joyce, "A method to determine acoustic properties of solids and its application to measuring oil film thickness in bearing shells of unknown composition," *Measurement*, vol. 195, p. 111176, May 2022, doi: 10.1016/j.measurement.2022.111176.
- [34] G. Nicholas, T. Howard, H. Long, J. Wheals, and R. S. Dwyer-Joyce, "Measurement of roller load, load variation, and lubrication in a wind turbine gearbox high speed shaft bearing in the field," *Tribol Int*, vol. 148, p. 106322, Aug. 2020, doi: 10.1016/j.triboint.2020.106322.
- [35] G. Nicholas, B. P. Clarke, and R. S. Dwyer-Joyce, "Detection of Lubrication State in a Field Operational Wind Turbine Gearbox Bearing Using Ultrasonic Reflectometry," *Lubricants*, vol. 9, no. 1, p. 6, Jan. 2021, doi: 10.3390/lubricants9010006.
- [36] W. A. Gray and R. S. Dwyer-Joyce, "In-situ measurement of the meniscus at the entry and exit of grease and oil lubricated rolling bearing contacts," *Front Mech Eng*, vol. 8, Nov. 2022, doi: 10.3389/fmech.2022.1056950.

- [37] P. Zheng *et al.*, "Ultrasonic reflection measured oil film thickness in the slipper bearings of an aviation fuel piston pump," *Mech Syst Signal Process*, vol. 220, p. 111696, Nov. 2024, doi: 10.1016/j.ymssp.2024.111696.
- [38] J. Zhu, X. Li, S. Beamish, and R. S. Dwyer-Joyce, "An ultrasonic method for measurement of oil films in reciprocating rubber O-ring seals," *Tribol Int*, vol. 167, p. 107407, Mar. 2022, doi: 10.1016/j.triboint.2021.107407.
- [39] M. M. Schirru, R. S. Mills, O. Smith, R. S. Dwyer-Joyce, and M. Sutton, "In situ Measurement of Journal Bearing Lubricant Viscosity by Means of a Novel Ultrasonic Measurement Technique Using Matching Layer," *Tribology Transactions*, vol. 61, no. 1, pp. 157–167, Jan. 2018, doi: 10.1080/10402004.2017.1285970.
- [40] V. Buckin and E. Kudryashov, "Ultrasonic Shear Wave Rheology of Weak Particle Gels," *Adv Colloid Interface Sci*, vol. 89–90, pp. 401–422, 2001, doi: 10.1016/S0001-8686(00)00060-9.
- [41] M. Milanese, F. Iacobazzi, M. Stark, and A. Risi, "Development of common rail lube oil injector for large two-stroke marine diesel engines," *International Journal of Engine Research*, vol. 23, p. 146808742110080, Mar. 2021, doi: 10.1177/14680874211008005.
- [42] A. Hunter, "Ultrasonic Measurements of the Strip Thickness, Lubricant Film Thickness, Roll Deflection and Roll Stress in the Roll Bite in the Cold Rolling of Steel," University of Sheffield, 2018.
- [43] M. Schoenberg, "Elastic wave behavior across linear slip interfaces," *J Acoust Soc Am*, vol. 68, no. 5, pp. 1516–1521, Nov. 1980, doi: 10.1121/1.385077.
- [44] R. S. Dwyer-Joyce, T. Reddyhoff, and J. Zhu, "Ultrasonic Measurement for Film Thickness and Solid Contact in Elastohydrodynamic Lubrication," *J Tribol*, vol. 133, no. 3, Jul. 2011, doi: 10.1115/1.4004105.
- [45] J. A. Cao-Romero-Gallegos, S. Taghizadeh, O. A. Aguilar-Rosas, R. S. Dwyer-Joyce, and L. I. Farfan-Cabrera, "The effect of electrical current on lubricant film thickness in boundary and mixed lubrication contacts measured with ultrasound," *Friction*, vol. 12, no. 8, pp. 1882–1896, Aug. 2024, doi: 10.1007/s40544-024-0890-7.